ESTIMATION OF THE PERSISTENT SCATTERER DENSITY USING OPTICAL REMOTE SENSING DATA AND LAND COVER DATA

Simon Plank[(1)], John Singer[(1)], Kurosch Thuro[(1)]

[(1)]Technische Universität München, Chair for Engineering Geology, Arcisstr. 21, 80333 München (Germany), Email: simon.plank@mytum.de, singer@tum.de, thuro@tum.de

ABSTRACT

In recent years persistent scatterer radar interferometry (PS-InSAR) has proven to be a powerful remote sensing technique to measure deformation of the Earth's crust with an accuracy of a few millimetres. However to ensure a PS-InSAR processing with useable results, a stack containing at least 30 to 50 radar images is required. This high amount of radar images is a very important cost factor when applying this method. In this paper we present two methods for estimating the density of scatterers (possible persistent scatterers) prior to the radar recording of the area of interest. The goal of this scatterer estimation is to find out, whether the scatterer density of a certain test site is high enough for PS-InSAR processing, or whether artificial scatterers, like corner reflectors, are necessary.

1. INTRODUCTION

Persistent scatterer radar interferometry (PS-InSAR) is a powerful remote sensing technique to measure deformation of the Earth's crust with an accuracy of a few millimetres [1][2][3]. But a high quality PS-InSAR processing is only possible with a stack containing at least 30 to 50 radar images (depending on the test site's land cover) [4]. This high amount of radar images is a very important cost factor when applying this method. Here we present two methods for estimating the density of possible persistent scatterers before the test site is recorded by radar. The goal of this scatterer estimation is to estimate, whether the scatterer density of the area of interest is high enough for PS-InSAR processing, or whether the scatterer density has to be artificially increased by corner reflectors – prior to the costly data acquisition.

The development of the scatterer density estimation methods is done empirically in a geographical information system (GIS) by comparing the distribution of real PS-targets (results of PS-InSAR processing) of several test sites with freely available (1) data of optical remote sensing sensors, such as Landsat and ASTER, and (2) land cover data, such as GlobCover, Corine and Africover.

Firstly, the optical remote sensing data were used to calculate the NDVI (Normalized Difference Vegetation Index) value of the test sites at various seasons. The paper shows a strong correlation of the NDVI value and the PS target distribution. Secondly, using the land cover data, the PS density of each single land cover class was calculated. To guarantee a wide usability of these methods, test areas with different types of land cover and of different climate were chosen. Therefore, both of the methods described above, enables the user to estimate the scatterer density (possible PS targets) before the area of interest is recorded by radar. The methods are intended for a first step evaluation whether the PS-InSAR technique can be applied for monitoring a certain test site. A great benefit of these methods is free availability and the (mostly) global coverage of the data used.

2. REFERENCE SAR DATA

To test the methods described below three datasets of geocoded PS-targets were available (Fig.1, Tab. 1). For the Cairo test site, Egypt (70 km x 45 km) the results of three PS detection methods were used: "Signal to clutter ratio" (SCR), "Thresholding on the amplitude dispersion" and the combination of both methods. The PS-targets were processed by using ENVISAT ASAR (Advanced Synthetic Aperture Radar, C-band) scenes.

The Aosta Valley test site, north-west Italy (130 km x 75 km) consists of two Radarsat-1 (C-band) footprints (each ascending and descending orbit). For this test site "normal" PS-targets and distributed scatterer (DS, SqueeSAR) were available [5].

For the Budapest test site, Hungary (13.4 km x 13.5 km) PS-targets of TerraSAR-X data were used.

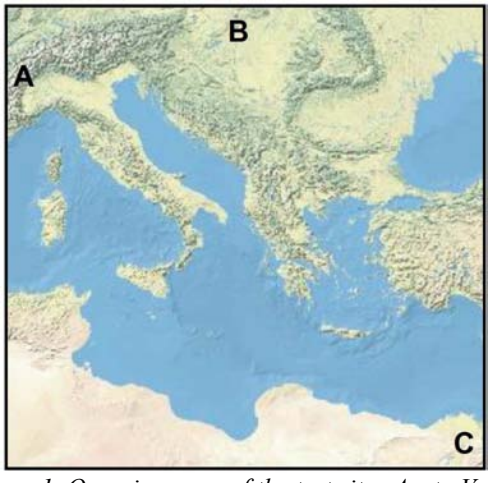

Figure 1. Overview map of the test sites Aosta Valley (A), Budapest (B) and Cairo (C)

Proc. 'Fringe 2011 Workshop', Frascati, Italy, 19–23 September 2011 (ESA SP-697, January 2012)

Table 1. Used PS-targets datasets

Test site	Satellite	Mode	Period
Cairo	ENVISAT	Image	2003-2009
Aosta Valley	Radarsat-1	Standard 3	2003-2010
Budapest	TerraSAR-X	StripMap	2008-2010

3. NDVI-PS-PERCENTAGE

3.1. Normalized difference vegetation index

The normalized difference vegetation index (NDVI) is a measure of the vegetation density of the test site. It can be calculated by using optical multispectral sensors working in the visible and near infrared (NIR) region of the electromagnetic spectrum [6][7][8]. Fig. 2 shows the spectral signatures of water, dry soil and vegetation. The NDVI uses the significant difference of the vegetation signature between the RED and NIR channel [9]. Eq. 1 shows the calculation of the NDVI. Being a ratio, the NDVI is independent on the illumination, atmospheric effects and topography. NDVI calculations of different acquisition times can be compared. The scale of the NDVI is form -1 to +1.

$$NDVI = \frac{NIR - RED}{NIR + RED} \quad (1)$$

As water has no reflection in infrared, its NDVI is -1. The NDVI value of bare areas (rock, sand and snow) is less than +0.1. PS-targets are limited to vegetation-free areas. The NDVI increases with denser vegetation (+0.2 to +0.3: grassland, shrubland; +0.6 to +0.8: forest).
Therefore the NDVI can be used to estimate the PS-density prior to the radar recoding the area of interest.

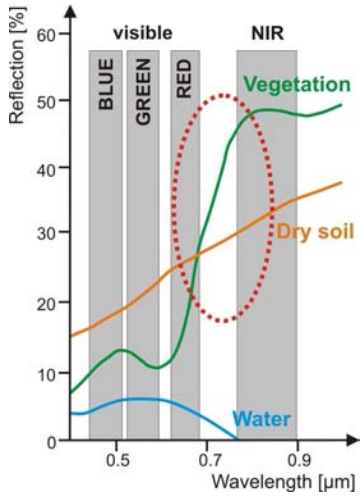

Figure 2. Spectral signatures of water, dry soil and vegetation in the visible and NIR region of the electromagnetic spectrum (grey boxes: Landsat bands) [9]

3.2. NDVI-PS-percentage: method

For all three test sites several free available Landsat ETM+ (Enhanced Thematic Mapper Plus, http://geo.arc.nasa.gov/sge/landsat/l7.html) and ASTER (Advanced Spaceborne Thermal Emission and Reflection Radiometer, http://asterweb.jpl.nasa.gov) data with 0 % cloud cover and from all seasons were chosen. The time period of the optical satellite data is equal to the acquisition time period of the SAR scenes (see section 2). Landsat and ASTER data are available at: http://glovis.usgs.gov.
Fig. 3 describes the procedure of the NDVI-PS-percentage calculation. For each single NDVI value the percentage of pixels with at least one PS target is calculated. This enables the calculation of the probability to find a PS-target at a specific NDVI value.

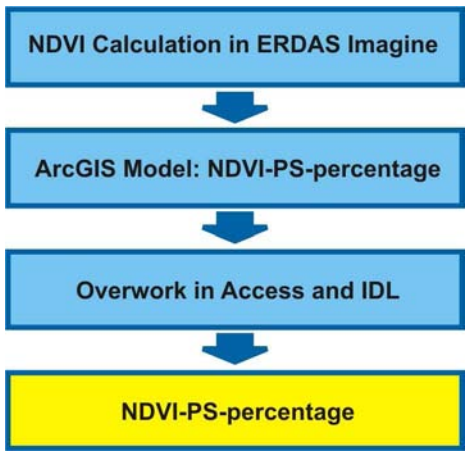

Figure 3. Procedure of the NDVI-PS-percentage method

3.3. NDVI-PS-percentage: results

Fig. 4 shows for each single NDVI value of the Cairo test site the percentage of pixels with at least one PS-target. The NDVI was calculated for six Landsat 7 scenes: March and May 2001, May and December 2002 and February and March 2003.
One can recognize two peaks. The first one ranges from NDVI -0.2 to 0.0 (for PS percentage > 5). This peak is formed by the Landsat scenes recorded in summer (March and May). The second peak (NDVI 0.0 to +0.16; for PS percentage > 5) is formed by the winter scenes (February and December).
The increase of the NDVI values from summer to winter can be explained by the desert climate of the Cairo test site. The precipitation and thereby the growing season is limited to the winter season. This causes an increase of the NDVI value in winter. As most PS-targets are surrounded by some vegetation, the growing of the vegetation causes an increase of the NDVI value of the pixel containing the PS-target.

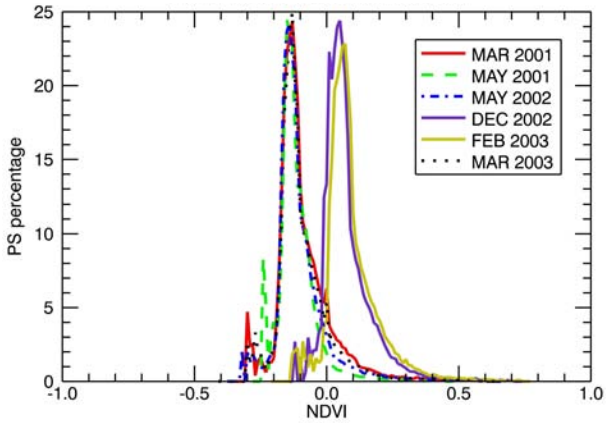

Figure 4. The Cairo test site: Percentage of NDVI values with at least one PS-target (Landsat 7 and ENVISAT ASAR)

The NDVI-PS-percentage methods works quite well at the Cairo test site, because of the spatial resolution of the used sensors (ENVISAT ASAR and Landsat 7) are the same (30 m) and wide areas of the test site are (almost) free of vegetation (especially the desert areas).

For the Budapest test site (Fig. 5) three cloud-free ASTER scenes of the same time period as the reference radar data were available: May 2008, October 2009 and June 2010. For the October scene the NDVI values ranges from -0.4 to +0.4 (for PS percentage > 5). The May and June graphs (-0.3 to +0.4) match very well and show a little higher NDVI values than the October graph (due to the higher vegetation density in summer).

The PS-targets of the Budapest test site were processed using TerraSAR-X StripMap Mode data (3 m spatial resolution). Furthermore, the majority of the scene is urban area. Therefore the number of PS targets is quite high. This explains the high PS percentage (up to 65) in the NDVI-PS-percentage graph (Fig. 5).

The widening of the NDVI-PS-percentage graphs of the Budapest test site are caused by the strong differences of the spatial resolution of ASTER (15 m) and TerraSAR-X (3 m).

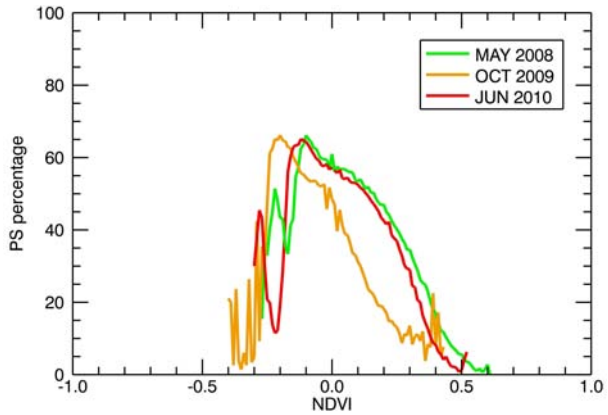

Figure 5. The Budapest test site: Percentage of NDVI values with at least one PS-target (ASTER and TerraSAR-X)

Fig. 6 shows the NDVI-PS-percentage of the Aosta Valley test site using four ASTER scenes recorded in May 2004, January 2006 and August and September 2009.

One can recognize a very wide scattering of the NDVI values. Considering only PS (& DS [5]) percentage greater than 5, one can recognize two peaks. The first one ranges from -0.27 to 0.0 (winter: January and May (mountainous terrain)) and the second one ranges from +0.13 to +0.55 (summer: August and September). Fig. 5 shows a very strong increase of the NDVI values from winter to summer because of the increase of the vegetation density (growing season is summer).

As large areas of the Aosta Valley test site are covered with dense vegetation (e.g. forest), the NDVI-PS-percentage graphs are widely scattered.

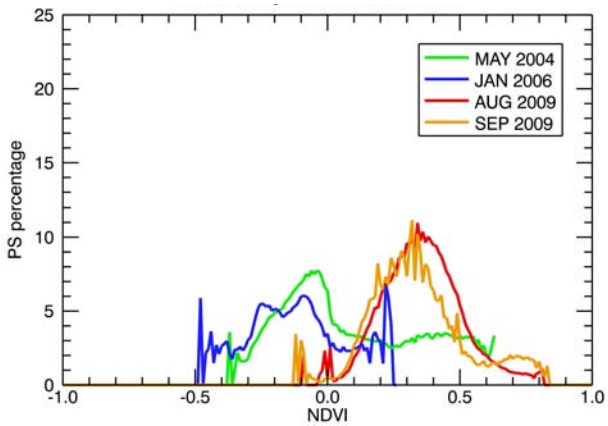

Figure 6. The Aosta Valley test site: Percentage of NDVI values with at least one PS (& DS) target (ASTER and Radarsat-1)

Fig. 7 shows the extreme case: a PS-target (one singe building) is surrounded by dense vegetation (e.g. forest). (All pixels around the illustrated one are dense vegetation). In a radar image in the pixel containing the building and forest the backscatter of the building dominates the surrounding vegetation. Therefore this pixel is a PS candidate (if it has a high coherence value). However, in an optical image the reflection of the sunlight from all objects within the pixel are averaged. Therefore the NDVI value of this pixel is almost as high as the NDVI values of the surrounding pixels (containing only dense vegetation).

Much better results of the NDVI-PS-percentage method – especially in test sites with dense vegetation and widely dispersed PS-targets – are expected with high resolution optical (multispectral) sensors, such as IKONOS, KOMPSAT-2 and WorldView-2. When using such high resolution sensors, the area around the PS-targets gets smaller. Consequently the NDVI of the pixels is mostly influenced by the PS-target and not by the surrounding vegetation.

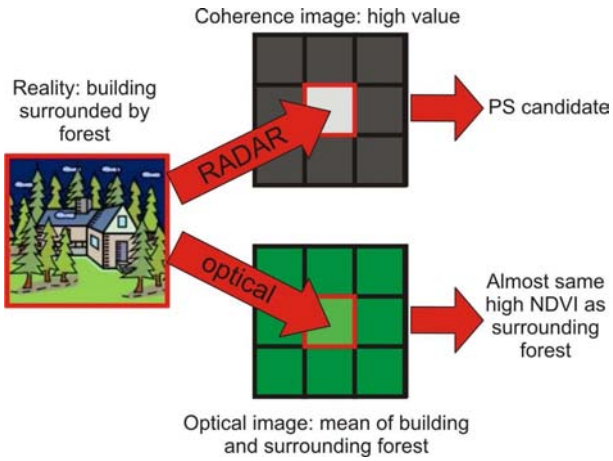

Figure 7. The different behaviour of optical and microwave (radar) sensor

4. LAND COVER PS

4.1. Freely available Land Cover data

The second method for PS density estimation prior to the radar recording of the area of interest uses freely available land cover data. The GlobCover land cover dataset has a global coverage and a spatial resolution of 300 m. It was derived by the classification of MERIS (Medium Resolution Imaging Spectrometer, ENVISAT sensor) data. 22 land cover classes are distinguished. GlobCover of the years 2005 and 2009 are available. More information about this land cover data can be found at: http://ionia1.esrin.esa.int/.

The year 2006 version of Corine (Coordination of Information on the Environment) land cover data has a spatial resolution of 100 m. Corine land cover is based on satellite data (scale 1:100,000). 47 land cover classes are distinguished. As the coverage of this land cover dataset is limited to Europe, it was used for the test sites Budapest and Aosta Valley. Corine 2006 is available at: http://www.eea.europa.eu.

For the Cairo test site the Africover land cover data was used. The source of this dataset are Landsat imagery (scale 1:100,000) which was acquired in 1997. More information about Africover is available at http://www.africover.org.

4.2. Land Cover PS: method

Using the land cover datasets described above, for each single land cover class the number of PS-targets lying inside the land cover class and the entire area of the class (within the test site) was calculated. Then the PS density (PS-targets per km²) was derived (Eq. 2).

$$PS\ density = Number\ of\ PS\ targets\ /\ Area\ of\ land\ cover\ class \quad (2)$$

After the calculation of the absolute PS density for all land cover datasets and test sites, the so called "relative PS density" was calculated. The absolute PS densities of all land cover classes were divided by the value of the reference class "urban area". Consequently the "relative PS density" of the reference land cover class "urban area" is "1". All land cover classes with a "relative PS density" greater than "1" have a higher absolute PS density and vice versa. Using the "relative PS density" one is able to compare PS-target datasets of different radar sensors (working with different wavelength, different imaging modes, etc.) processed with different PS detection methods and algorithms.

4.3. Land Cover PS: results

Fig. 8 shows the results of the "relative PS density" calculation for the test sites Cairo, Budapest and Aosta Valley. The upper graph of Fig. 8 shows the results for the GlobCover land cover dataset with a spatial resolution of 300 m. As this dataset has a global coverage, all three test sites can be considered in the calculations. The lower graph of Fig. 8 only considers the European test sites, Budapest and Aosta Valley, as the Corine land cover data has only Europe wide coverage. The Corine land cover dataset has a higher spatial (100 m) and thematic resolution (more different land cover classes) than GlobCover.

As the Aosta Valley test site is in mountainous area, layover and shadowing influence the application of PS-InSAR. To take this influence in account, we calculated an additional "relative PS density" dataset with layover and shadowing areas excluded (marked as "layover excluded" in Fig. 8). The layover and shadowing areas were simulated using the method described in [10].

For both land cover datasets "urban area" is used as reference class (marked red in the graphs) and set to a "relative PS density" of "1". To be able to compare the Corine 2006 and the GlobCover land cover datasets, the Corine class "discontinuous urban area" is chosen as reference class, as it best matches with the GlobCover class "urban area" (based on legend description).

Both graphs in Fig. 8 show that most of the land cover classes have a lower "relative PS density" than the reference class "urban area". Exceptions are the classes "continuous urban area" and "road and rail road" (both Corine 2006) and "bare areas" (for "msr" and "cat" Cairo in the GlobCover dataset, Fig. 8). As in Corine class "continuous urban area" the density of building is higher and the vegetation density is lower than in class "discontinuous urban area", also the "relative PS density" of the first one is higher.

The "relative PS density" values of the different test sites show mostly a good conformity inside one land cover class.

The value for Corine class "continuous urban area" of test site Budapest is ca. 33 % higher than the corresponding values of test site Aosta Valley. The reason for this is the very high spatial resolution of the radar data used for the PS processing at the Budapest test site (TerraSAR-X StripMap, 3 m spatial resolution) in com-

parison to the Radarsat-1 data of test site Aosta Valley (27 m spatial resolution). Due to the very high spatial resolution of the TerraSAR-X data, the absolute PS density and therefore also the "relative PS density" is very high for densely built-up areas.

The GlobCover land cover class "bare areas" show very high differences between the test sites Cairo and Aosta Valley. Due to the small number of land cover classes, GlobCover contains the desert areas of Cairo and bare rock areas of Aosta Valley in the same land cover class: "bare areas". Both test sites have a very different climate. Due to the very low annual precipitation (29 mm/a), the vegetation-free stony and rocky desert of the Cairo test site has ideal properties to form PS-targets (high coherence). As opposed to this, the "bare areas" of the Aosta Valley test site are highly elevated mountainous areas (→ layover and shadow areas) with very high annual precipitation (1863 mm/a) and also small parts of sparsely vegetation. Therefore the "bare areas" of the Aosta Valley test site are not as suitable for PS-InSAR as the "bare areas" of the Cairo test site.

As already mentioned in section 4.2., the "relative PS density" is independent of the used radar sensor, imaging mode, PS detection, PS-InSAR processing algorithm, etc. The idea of the "relative PS density" method is to be able to estimate the absolute PS density of all land cover classes within the test site, prior to radar recording. Precondition for the "relative PS density" method is the known absolute PS density in "urban area" for a test site of the same climate zone and which was acquired and processed with the same, respectively comparable radar sensor and PS-InSAR algorithm.

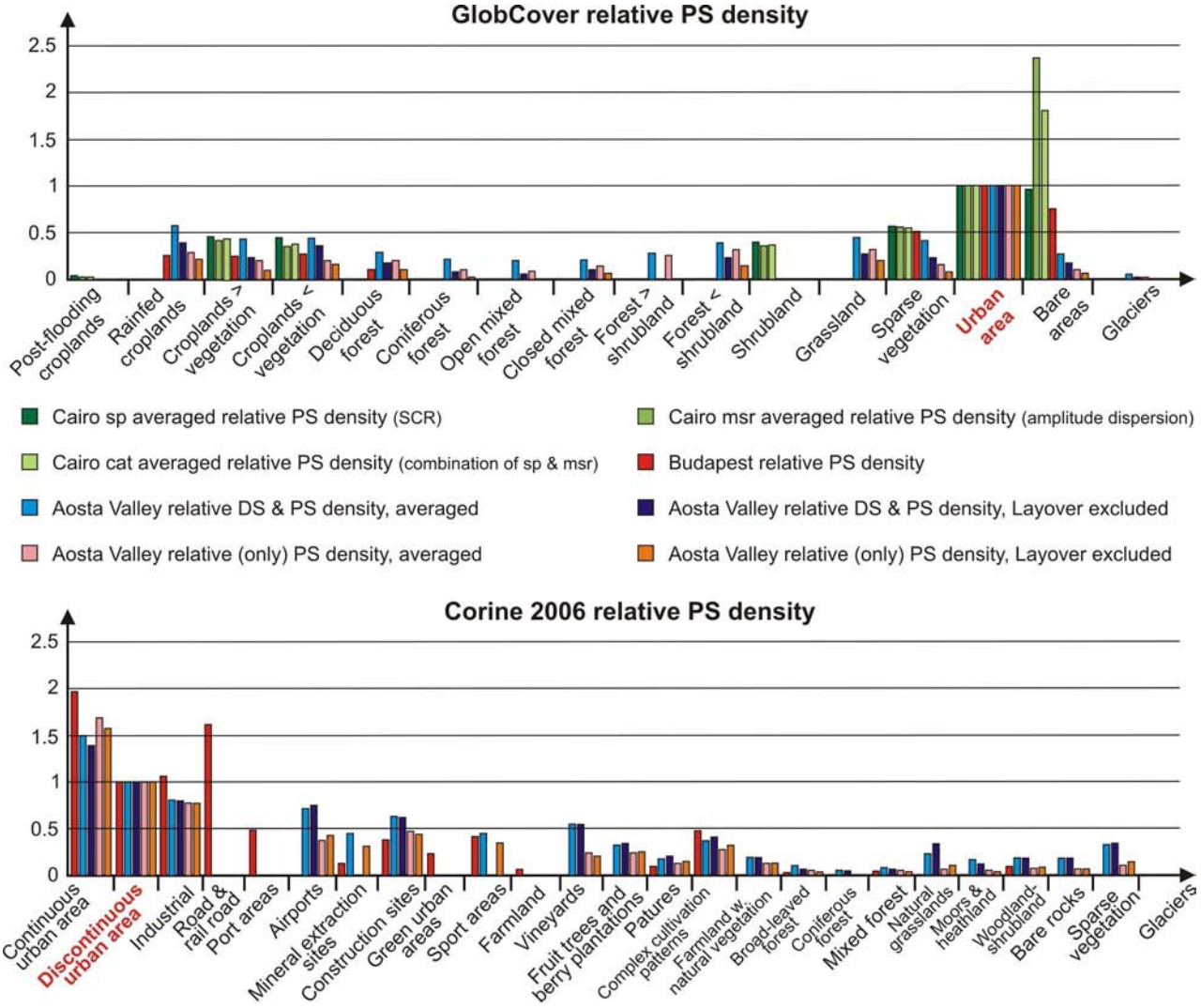

Figure 8. The "relative PS density" of different land cover classes for the test sites Cairo, Budapest, Aosta Valley. Top: GlobCover land cover; bottom: Corine 2006 land cover

Due to its higher spatial and thematic resolution the Corine land cover is better suited for the "relative PS density" method than the GlobCover dataset. However, as in some areas only GlobCover is available, it was also considered in our studies. The best results can be expected when using the land cover data with the highest spatial (and thematic) resolution that is available for the test site. It is also very important to use a land cover dataset that considers the specific climate conditions of the area of interest.

5. CONCLUSION

In this paper we presented two methods for estimating the persistent scatterer (PS) density, prior to the radar recording of the area of interest.
The first method uses the normalized difference vegetation index (NDVI) calculated out of free available optical satellite data (Landsat and ASTER). For each single NDVI value the percentage of pixels with at least one PS-target is calculated. The results showed that this method works quite well in test sites dominated by sparsely vegetated areas (e.g. test site Cairo). For test sites with dense vegetation (e.g. Aosta Valley), we expect much better results when using high resolution optical sensors. This will be part of our future work.
The second method for the PS density estimation uses free available land cover data (e.g. GlobCover and Corine 2006). The results of the described "relative PS density" method are independent of the used radar sensor, imaging mode and PS processing algorithm.

6. ACKNOWLEDGEMT

The authors would like to thank Dr. Alessandro Ferretti (Tele-Rilevamento Europa - T.R.E), Dr. Michael Riedmann and Dr. Oliver Lang (both Astrium Infoterra) and Dr. Michael Foumelis (University of Athens) for providing the PS-targets data of the test sites.
We thank the Universität Bayern e.V. and the Technische Universität München Graduate School for financial support.

7. REFERENCES

1. Kampes, B. (2006). *Radar Interferometry*. *Persistent Scatterer Interferometry*, Springer, Dordrecht, The Netherlands, 211 pp.

2. Massironi, M., Zampieri, D., Bianchi, M., Schiavo, A. & Franceschini, A. (2009). Use of PSInSAR^{TM} data to infer active tectonics: Clues on the differential uplift across the Giudicarie belt (Central-Eastern Alps, Italy), *Tectonophysics*, **476**, 297-303.

3. Vilardo, G., Ventura, G., Terranova, C., Matano, F. & Nardo, S. (2009). Ground deformation due to tectonic, hydrothermal, gravity, hydrogeological, and anthropic processes in the Campanie Region (South Italy) from Permanent Scatterer Synthetic Aperture Radar Interfeormetry, *Remote Sensing of Environment*, **113**, 197-212.

4. Ferretti, A., Prati, C. & Rocca, F. (2000). Analysis of Permanent Scatterers in SAR Interferometry, In Proc. IGARSS 2000, 761-763.

5. Ferretti, A., Fumagalli, A., Novali, F., Prati, C., Rocca, F. & Rucci, A. (2011). A New Algorithm for Processing Interferometric Data-Stacks: SqueeSAR, IEEE Trans. Geosci. Remote Sens.,**99**, 1-11.

6. Lillesand, T.M. & Kiefer, R.W. (2000). *Remote Sensing and Image Interpretation*, 4th Edit., John Wiley & Sons, New York, USA, 724 pp.

7. Albertz, J. & Wiggenhagen, M. (2009). *Guide for Photogrammetry and Remote Sensing*, 5th Edit., Wichmann, Paderborn, Germany, 334 pp.

8. Hildebrandt G. (1996). *Fernerkundung und Luftbildmessung*, Wichmann, Reinheim, Germany, 676 pp.

9. Hoffer, R.M. (1978). Biological and Physical Considerations in applying Computer-Aided Analysis Techniques to Remote Sensor Data. In *Remote Sensing: The Quantitative Approach* (Eds. P.H. Swain & S.M. Davis), McGraw-Hill, New York, USA, pp227-289.

10. Plank, S., Singer, J., Minet, Ch. & Thuro, K. (2010). GIS based suitability evaluation of the differential radar interferometry method (D-InSAR) for detection and deformation monitoring of landslides. In Proc. of the FRINGE 2009 Workshop (Ed. H. Lacoste), ESA SP-667 (CD-ROM), ESA Publication Division, European Space Agency, Noordwijk, The Netherlands.